MR-Based Detection of Individual Histotripsy Bubble Clouds Formed in Tissues and Phantoms

Steven P. Allen[1] *, Luis Hernandez-Garcia[2], Charles A Cain[1, 3] Timothy L. Hall[1, 3]

1. Department of Biomedical Engineering, University of Michigan, USA
2. fMRI Laboratory, Department of Biomedical Engineering, University of Michigan, USA
3. Authors Charles Cain and Timothy Hall have equity, royalty, and consulting interests in HistoSonics, Inc.

*Department of Biomedical Engineering

University of Michigan

2131 Gerstacker

2200 Bonisteel, Blvd.

Ann Arbor, MI 48109-2099

Word count: 4309

Key Words: Histotripsy, Cavitation, Focused Ultrasound Surgery, Tissue Erosion, Tissue Homogenization, Intravoxel Incoherent Motion.

Abstract

Purpose

To demonstrate that MR sequences can detect individual histotripsy bubble clouds formed inside intact tissues.

Methods

A line-scan and an EPI sequence were sensitized to histotripsy by inserting a bi-polar gradient whose lobes bracketed the lifespan of a histotripsy bubble cloud. Using a 7T, small-bore scanner, these sequences monitored histotripsy clouds formed in an agar phantom and in vitro porcine liver and brain. The bipolar gradients were adjusted to apply phase with k-space frequencies of 10, 300 or 400 cm^{-1}. Acoustic pressure amplitude was also varied. Cavitation was simultaneously monitored using a passive cavitation detection (PCD) system.

Results

Each image captured local signal loss specific to an individual bubble cloud. In the agar phantom, this signal loss appeared only when the transducer output exceeded the cavitation threshold pressure. In tissues, bubble clouds were immediately detected when the gradients created phase with k-space frequencies of 300 and 400 cm^{-1}. When the gradients created phase with a k-space frequency of 10 cm^{-1}, individual bubble clouds were not detectable until many acoustic pulses had been applied to the tissue.

Conclusion

Cavitation-sensitive MR-sequences can detect single histotripsy bubble clouds formed in biologic tissue. Detection is influenced by the sensitizing gradients and treatment history.

Key Words: Histotripsy, Cavitation, Focused Ultrasound Surgery, Tissue Erosion, Tissue Homogenization, Intravoxel Incoherent Motion.

Comment [SPA1]: Changes made in response to comment 3 by Referee 1.

Introduction

Mechanical disruption of tissue through ultrasonic cavitation (histotripsy) has shown promise as a non-invasive, transcranial and transcostal soft-tissue ablation surgery (1–5). In both the transcostal and transcranial cases, histotripsy produces predictable, confined lesions with sharp borders, mainly because the size and location of bubble clouds formed by the ultrasonic pulses can be controlled even when the sound field is distorted by bone (1–3). Further, these bubble clouds can be produced using ultrasound pulsing schemes with very low duty cycles, leading to negligible heating in soft tissues and bone (2).

For safety reasons, transcostal and transcranial ablation must be coupled with an imaging system capable of localizing histotripsy bubble clouds formed at the onset of therapy, prior to irreversible ablation. This allows the operator to terminate therapy should the bubble cloud be formed in a sensitive structure. Nominally, acoustic cavitation detection achieves this purpose (6–8). However, in the transcostal and transcranial cases, acoustic cavitation detection cannot reconstruct the bubble cloud without making some correction for field aberrations imposed by the overlying bone (6,9). To this end, the patient, prior to therapy, submits to computed tomography (10) or ultra-short echo time MR imaging (11) to characterize her bone structure. Then, during therapy, the operator must rely on both these scans and a computational model to correct the cavitation detection signals (12). The additional cost, risk, and complexity of this step could be avoided by using an imaging method that can both be sensitized to the bubble cloud and produce accurate anatomical images without needing aberration correction.

Previous developments of MRI-based bubble detection for focused ultrasound surgeries have concentrated on either detecting cavity voids formed during boiling (13,14) or detecting changes in T2* (15–18). These methods are unsuitable for monitoring histotripsy because they require the bubbles to persist through most of the acquisition time. Histotripsy bubble clouds have a lifespan of hundreds of microseconds and collapse too quickly to be directly picked up by even the fastest of MR sequences.

Recently, a magnetic resonance imaging technique has been developed to detect the incoherent water motion caused by inertial cavitation (19,20). This can be accomplished by synchronizing the ultrasound pulses with a bipolar, motion-encoding gradient. With the gradients in place, the water flow generated by cavitation disrupts the ability of the second gradient lobe to rewind linear phase

imposed by the first gradient lobe. Images produced from these sequences show signal loss localized at the cavitation site. Though this method can easily detect bubble clouds made in free fluid and in tissue that has already been homogenized, it is uncertain if it can be used to detect histotripsy at the onset of therapy, where the intact tissue may inhibit both the expansion of the bubble cloud as well as subsequent water motion.

In the following paper, we assume that, when the distance between phase wraps introduced by the first lobe of the encoding gradient nears the size of the water perturbation made by the bubble cloud, the second gradient lobe is then unable to rewind the phase imposed by the first. This will result in signal loss localized to the cavitation site. Thus, very small bubble clouds can be visualized when the sensitizing gradients extend into regions of k-space with high spatial frequencies. Sequences where the gradients extend only into low spatial frequency regions will be unable to detect small bubble clouds.

We aim to demonstrate that MR pulse sequences with sensitizing gradients that extend into high k-space frequencies can capture the first bubble clouds formed inside a tissue target. Sequences that extend only into low frequency k-space will not be able to capture the first bubbles formed in a tissue target. For this investigation, we develop single-shot, line-scan and EPI imaging sequences that are sensitized to histotripsy. The contribution of non-cavitation based fluid flow is investigated by using the line-scan sequence to estimate the cavitation pressure threshold in an agar phantom. We then use both sequences to monitor a series of bubble clouds formed in in-vitro porcine liver and brain samples.

Methods

Transducer

Our experiments were conducted using a custom-made, MR-compatible transducer placed in the bore of a 7T-310, small animal scanner (Agilent, Walnut Creek, CA) capable of gradients up to 400 $mT\ m^{-1}$. This transducer was composed of 16 focused elements, each with a center frequency of 500 kHz and arrayed along the surface of a sphere subtended by 1.84 steradians. The array had a focal depth of 56 mm and an aperture diameter of 115 mm. After construction, the transducer was calibrated using a fiber-optic hydrophone (21) using the same methods discussed in (22) and was found to generate peak negative pressures exceeding 28 MPa. The -6dB axial and longitudinal beam widths were found to be 2.1 mm and 7.0 mm. The acoustic pulses were 4.5 μs long and contained roughly two full cycles. The driving system of this transducer was activated by the MR controller console using programmable trigger pulses.

Comment [SPA2]: Changes made in response to comment 5 by Referee 1.

One element in the transducer was wired as a send-receive hydrophone capable of recording acoustic emissions from cavitation activity. The voltage waveforms captured by this element were recorded by an oscilloscope (Pico Technology, Cambridgeshire, UK) and used for passive cavitation detection (PCD). In experiment (A) below, cavitation activity was determined by first subtracting an estimate of the reflections of the acoustic pulse off the transducer cap and then integrating the magnitude of the remaining backscatter signal over a period corresponding to 75 to 90 μs after the acoustic pulse had been fired. The 75 to 90 μs period corresponds to the time it takes for the acoustic pulse to travel to the focus and back. Details for this calculation are given under the section titled Experiment A. In experiment (B), cavitation activity was estimated by integrating the magnitude of the acquired PCD signal over the same period as in experiment (A).

The transducer was connected to a cap such that its cavity could be filled with degassed saline and coupled to a tissue sample placed at the transducer focus. A surface coil was then placed about the sample and centered on the cavitation site. See Fig. 1.

MRI Sequence

MR images were acquired using either a modified spin-echo, line-scan (23) sequence or an EPI sequence as shown in Fig. 2. In both the line-scan and the EPI sequence, a bipolar gradient was placed about a single ultrasound pulse such that one bubble cloud formed and collapsed between

the gradient lobes. The time between the gradient lobes was limited to at most 1 ms. The durations of the acoustic pulse (~ 5 μs) and the lifecycle of the bubble cloud (~200 μs) were short enough to thoroughly mix water before the second gradient lobe rewound the phase imposed by the first. Repeating this sequence simultaneously applied consecutive histotripsy pulses to a target and acquired cavitation-sensitive images of each bubble cloud.

For the spin-echo, line-scan sequence, the slice-select gradient for the refocusing pulse was rotated to play along the phase-encode axis. As a result, the excitation planes intersected in a 1.5 mm rectangular beam that transected the transducer focus, parallel to the readout direction. The phase-encode gradient was also removed. Fourier transforming the resulting spin-echo yielded a single 1-D "image" of a column of tissue. Line-scanning allowed extremely fast sampling of the histotripsy process at the cost of losing spatial information in the phase encode direction.

Comment [SPA3]: Changes made in response to comment 6 by Referee 1.

Fig. 3 indicates how the refocusing pulse was ensured to transect the transducer focus. A sacrificial sample was placed in the transducer focus and imaged using a spin-echo sequence (Frame A). Then, a cavitation-sensitized 2D sequence (19) was used to plan the location of the rotated refocusing pulse (Frames B-C). In the resulting 1D images (Frame D), cavitation caused observable signal loss. The parameters used in this figure are TR = 1.2 s, TE = 65 ms, FOV = 25 x 25 mm, matrix = 125 x 125, bandwidth = 30.5 kHz, and NEX = 1. Sensitizing gradient amplitude, separation, and duration are identical to that used in experiment A.

Throughout the experiments described below, instances of the histotripsy imaging sequence were interleaved with an identical sequence but with the ultrasound system deactivated. For these cases, a bubble cloud did not form between the sensitizing gradients, resulting in images of the tissue target interleaved between every two acoustic pulses. These images were used as a control against which we could compare the signal loss caused by the bubble cloud.

The k-space frequency created by the sensitizing gradients of the MR sequence was controlled by increasing or decreasing the amplitude of the motion encoding gradients while keeping the duration of the lobes and the period between them constant.

Comment [SPA4]: Changes made in response to comment 3 by Referee 1.

For experiment (A), the imaging parameters for the line-scan sequence were TR = 1 s, TE = 41 ms, FOV = 25 x 1.5 x 1.5 mm, matrix = 125 x 1 x 1, bandwidth = 30.5 kHz, and NEX = 1. The

sensitizing gradient lobes were each 2 ms long, separated by 1 ms and played at an amplitude of 117.8 $mT\ m^{-1}$, leading to a b-value of 9.2 $s\ mm^{-2}$ and a k-space frequency of 100 cm^{-1}.

For experiment (B), the imaging parameters for the line-scan sequence were: TR = 0.65 s, TE = 35 ms for the liver samples and TE = 50 ms for the brain samples, FOV = 25 x 1.5 x 1.5 mm, matrix = 75 x 1 x 1, bandwidth = 30.5 kHz and NEX = 1. The sensitizing gradient lobes were each 2.5 ms long and separated by 1 ms. While scanning six liver samples and six brain samples, the gradient amplitudes were set to 9 $mT\ m^{-1}$, leading to a b-value of 0.1 $s\ mm^{-2}$ and a k-space frequency of 10 cm^{-1}. While scanning another set of six liver and six brain samples, the amplitude was set to 376 $mT\ m^{-1}$, leading to a b-value of 171 $s\ mm^{-2}$ and a k-space frequency of 400 cm^{-1}.

Imaging parameters for the EPI sequence were TR = 0.7 s, TE = 26 ms, FOV = 25 x 25 x 1 mm, matrix = 64 x 64 x 1, bandwidth = 360 kHz, shots = 2, k-zero = 16, and NEX = 1. The sensitizing gradient lobes were each 4 ms long, separated by 0.5 ms, and played at an amplitude of 176 $mT\ m^{-1}$, leading to a b-value of 113 $s\ mm^{-2}$ and a k-space frequency of 300 cm^{-1}.

Comment [SPA5]: Changes made in response to comment 5 by Referee 1.

Comment [SPA6]: Changes made in response to comment 5 by Referee 1.

Comment [SPA7]: Changes made in response to comment 5 by Referee 1.

Comment [SPA8]: Changes made in response to comment 5 by Referee 1.

Comment [SPA9]: Changes made in response to comment 5 by Referee 1.

Comment [SPA10]: Changes made in response to comment 5 by Referee 1.

Comment [SPA11]: Changes made in response to comment 5 by Referee 1.

Comment [SPA12]: Changes made in response to comment 5 by Referee 1.

Experiment A: Determining Cavitation Threshold

Though the MR sequences were created to observe histotripsy cavitation, it is possible other effects such as streaming and motion caused by the acoustic radiation force may contribute to signal loss at the transducer focus. In the following experiment, we attempted to isolate the contribution of these effects by using both the MR line-scan sequence as well as the PCD system to determine the cavitation threshold pressure in a phantom. If present, both radiation force based water flow and streaming would cause the MR-sequence to detect motion at pressures below the cavitation threshold, leading to a threshold estimate that is lower and less sharp than that determined by the PCD system.

Experiment A was performed by placing a 1.5 cm wide by 2.5 cm long cylinder of 1.25% agar gel (LabScientific, Catalog# AG-SP) into the transducer focus. Agar phantoms at this concentration have acoustic attenuation near that of water (24).

A small liquefied volume was first created within the gel matrix prior to experimentation by applying a pre-treatment of one thousand histotripsy pulses at 35 MPa estimated peak negative pressure such that the physical environment would be consistent throughout the experiment. After pre-treatment, the line-scan imaging sequence was used to apply and image 100 histotripsy pulses all with a

common acoustic amplitude. This experiment was repeated 14 times while the acoustic output was ramped from 17 to 35 MPa at 14 discrete points.

The probability of stimulating a bubble cloud using an acoustic pulse with a given peak negative pressure was calculated by counting the fraction of pulses per acoustic amplitude where signal loss greater than a threshold value was observed. Signal loss was determined by dividing the signal at the focus in the histotripsy image by the signal at the focus in the corresponding control image. The baseline was determined by selecting a region of the phantom 2 mm away from the focus, where the signal appeared to remain constant over the entire experiment. The mean histotripsy image signal in this region was divided by the corresponding mean control image signal. A cavitation event was recorded when the signal loss at the focus for a given image fell below the baseline value by more than 5 standard deviations.

Simultaneous to this experiment, the PCD receiver recorded the acoustic emissions at the focus of the transducer. These waveforms were composed mainly of the acoustic pulse as it reflected off of the various surfaces within the experimental setup and, when present, cavitation emissions and cavitation backscatter. The cavitation threshold was computed by first subtracting the contributions made by reflections from each recorded waveform. These contributions were expected to vary linearly with increasing pressure amplitude. They were estimated by first averaging together the 100 waveforms recorded at 24 MPa and then averaging together the 100 waveforms recorded at 25 MPa and then multiplying the difference between these two averaged waveforms by each pressure level. A cavitation event was recorded when the integral of the magnitude of the signal remaining after subtraction exceeded the average integral value at 25 MPa by more than 5 standard deviations.

Experiment B: Tissue Treatment

The 1-D spin-echo sequence was used to monitor therapy in 12 in-vitro porcine liver and 12 in-vitro porcine brain samples harvested from a nearby slaughterhouse. Within twenty-four hours, the tissues were cut into pieces, immersed in degassed saline and held under -15 mm mercury vacuum for two additional hours. Liver pieces were cut from the edges of each liver lobe where blood vessels were the smallest. Brain pieces were cut from nearly every portion of the brain except for the brain stem. Typical attenuation coefficients for liver and brain range between 0.5 and 0.6 dB cm^{-1} MHz^{-1} (24). After being held in vacuum, the samples were placed in 1.5 cm wide by 2.5 cm long cylindrical

molds and covered in 2% agar. After gelation, each agar-sample construct was removed from its mold and placed in the transducer focus.

Tissue samples were treated with 800 histotripsy pulses using the line-scan sequence. Six liver and six brain samples were imaged using the high k-space frequency sequence while the other six liver and six brain samples were imaged using the low k-space frequency sequence. The histotripsy pulses had an estimated peak negative pressure of 35 MPa. One additional sample of brain tissue was imaged with the EPI sequence, applying 400 histotripsy cavitation pulses interleaved with 400 control images.

Throughout each experiment, the PCD system collected time-voltage waveforms proportional to the acoustic pressure incident on the receiver.

The signal losses induced by individual bubble clouds were extracted from the histotripsy images by averaging the pixels of each image that lay within a region of interest (ROI) set about the transducer focus. For comparison across tissue samples, each series of these values was then normalized to the signal level at the transducer focus prior to therapy. We then used the same method to extract any changes in the MR signal of the tissue as observed by the control images.

In order to quantify the observability of the bubble clouds, we estimated the minimum pulse number where the bubble cloud demonstrated at least a 50% chance of being observed. This was calculated by finding the smallest pulse number applied to six samples with a common k-space frequency and tissue type, where at least three of the six samples demonstrated a contrast-to-noise ratio (CNR) above 5. CNR was calculated by subtracting the mean focal signal of the histotripsy image from that of the preceding control image and then dividing by the standard deviation of the signal from a region outside the extent of the tissue sample.

Results

Experiment A: Cavitation Detection in Gel

The pressure-probability results produced by both the PCD and MRI systems as well as sigmoid functions fitted to these results are plotted in Fig. 4. The fit to the PCD data indicates a 0.5 cavitation probability threshold at 26.4 MPa peak negative pressure. The fit to the MRI data indicates a threshold at 26.6 MPa peak negative pressure. Pulses with pressures at or above 27 MPa produced significant MR-signal loss at least 90% of the time.

Experiment B: Tissue Treatment

The mean and standard deviation of the cavitation sensitized signal at the transducer focus for each tissue type and k-space frequency are plotted as a function of pulse number and displayed in Fig. 5.

By the end of therapy, all 24 tissue samples displayed cavitation induced signal loss with a CNR of at least 5. However, the point at which cavitation specific contrast became differentiable from the control signal varied with the sensitivity of the imaging sequence. When imaged with a k-space frequency of 400 cm^{-1}, the first histotripsy pulses applied in liver generated signal loss greater than 40 %. With each successive pulse, the MR signal continued to decrease until it reached a baseline at about 25% of the control signal, where it remained until completion of therapy. The noise floor across the experiments varied between 3 and 12%. For these tissue samples, 0.5 probability of detection was achieved by the 5^{th} pulse.

In brain, when imaged with a k-space frequency of 400 cm^{-1}, the very first histotripsy pulse attenuated the signal between 60% and 80 % and always produced a CNR above 5. Like the liver case above, the MR signal continued to decrease until it reached a baseline at about 25% of the control signal, where it remained until completion of therapy. For these tissue samples, 0.5 probability of detection was achieved by the 1^{st} pulse.

The cavitation sensitized signal in tissue samples imaged with a k-space frequency of 10 cm^{-1} did not produce a detectable amount of contrast until several pulses into treatment. The brain tissue samples demonstrated 0.5 probability of at the 15^{th} pulse while the liver tissue samples demonstrated 0.5 probability of detection at the 63^{rd} pulse.

In both brain and liver tissues scanned at low spatial frequency encoding, the cavitation sensitized signal reached a steady state of about 50% of the control signal, as opposed to the 25% signal level of the high spatial frequency encoding case.

Comment [SPA13]: Changes made in response to comment 4 by Referee 1.

By the end of therapy, the control signal in all 12 liver samples was 1.5 to 2.5 times greater than it was at the start of therapy. Further, this difference was at least 10 times larger than the noise floor. The control signal in all 12 brain samples did not demonstrate a significant change over the course of treatment.

The PCD signal displayed consistent levels across all histotripsy pulses in all the tissue experiments.

2D Imaging

The first images taken with the 2D EPI sequence are displayed in Fig. 6 and corroborate with the 1D-line-scan results. The sample, imaged at k-space frequency of 300 cm^{-1}, displays cavitation specific contrast within the first two acoustic pulses.

Discussion

Cavitation Detection without a Gel Matrix

The MRI and PCD sequence indicated a 0.5 probability threshold within 0.2 MPa of each other. Further, both threshold values are within one MPa to thresholds reported in the literature (25,26).

At pressures below 32 MPa, the MR sequence reports about 10% fewer cavitation events than the PCD system. This is possibly because the acoustic pulses at pressures below 32 MPa produced small bubble clouds. Unlike the PCD system, the MR line-scan sequence is subject to partial volume effects. Bubble clouds that cause motion outside the intersection of the two excitation planes, or bubble clouds that cause incoherent motion in a sub-voxel volume, will less effectively generate MR signal loss but will still be detected by acoustic methods.

Detecting the First Bubble Cloud in Tissue

The results shown in Fig. 5 confirm our hypothesis that the initial bubble clouds formed in tissues can be detected using MRI sequences. The very first cloud formed in brain tissue is consistently detectable. Meanwhile, in the liver, the bubble cloud is consistently detectable by the 5^{th} pulse. Further, the PCD signal remained quite uniform across all pulses in all the tissue experiments, indicating that the cavitation behavior did not change in a systematic manner during treatment.

It is currently unclear if applying 1 histotripsy pulse in the brain or 5 pulses in the liver will cause irreversible damage. Previous studies have indicated that small pulse numbers of histotripsy in rabbit kidney create scattered foci of hemorrhage and cell debris (27,28). But it is unknown if this trend continues in the brain and liver, or even if these organs will recover from such damage.

It appears from Fig. 5 that, with a k-space frequency of 400 cm^{-1}, the first bubble cloud formed in liver causes less signal attenuation than the first cloud formed in brain. This may be due to the liver being a stiffer tissue than the brain, leading the bubble cloud to have more difficulty driving flow. Scans at higher sensitivities or higher resolutions may better observe the first bubble cloud formed in liver.

For therapy in very stiff media such as fibrotic tissue, achieving sufficient resolution and sensitivity to visualize the bubble cloud will likely require trade-offs between imaging time, resolution, and image fidelity. In addition, the waveforms in the high sensitivity cases of this study already have b-

values above 100 s mm^{-2}, resulting in images moderately sensitive to thermal diffusion. Further increases in cavitation sensitivity will produce images even more sensitive to non-cavitation related sources of motion.

Lesion Monitoring Through Cloud Detection

Images acquired with low sensitivity to cavitation do not immediately produce statistically significant signal loss. However, as successive pulses are applied to the tissue, the bubble cloud becomes more apparent. We suspect this behavior is an indication of disruption of the tissue. As the cellular structure breaks down, there will be less resistance to flow at the focus, leading to more signal attenuation. If this is true, it may be possible to use cavitation sensitized MR sequences to monitor the progression of the histotripsy lesion. One may be able to choose an imaging sensitivity such that contrast is saturated once the lesion reaches a desired state of homogenization.

Lesion Monitoring Through T2-Weighted Imaging.

By the end of treatment, the control signal of each liver sample demonstrates 1.5 to 2.5 times more amplitude at the end of treatment compared to the beginning, with this difference in signal being at least 10 times larger than the noise floor. The majority of the signal increase occurs in the first 200 pulses, with diminishing gains for every pulse after that. This trend of an initial rapid increase in contrast followed by more gentle, asymptotic changes is also found in studies of other measures of histotripsy lesions such as acoustic backscatter reduction in kidney (27), Young's modulus in liver (29), color Doppler ultrasound (30), and optical measurements (31). Preliminary studies have found some correlation between T2 elevation and liver tissue homogenization (2,3,32–35). It is currently unclear why T2 weighted contrast in brain do not change in response to homogenization.

Real Time 2D Targeting and Monitoring

The images in Fig. 6 suggest that the principles behind 1D MR-based cavitation detection can be extended to 2D imaging. The EPI sequence is able to detect and localize the first two bubble clouds formed in the target.

In a clinical setting, the location of the transducer focus may not be precisely known. It may be more preferable to use 2D and 3D imaging sequences to localize the first histotripsy bubble clouds applied to the target. In addition, many clinical systems do not have the same field strength and gradient capability as the 7T scanner used here. Operating with reduced maximum gradient amplitudes,

reduced slew rates, and reduced signal-to-noise ratios may hinder detecting the first bubble clouds formed in tissues. Further adaptations, such as longer gradient times, pulsing to multiple locations during a single acquisition or modifying the pulsing parameters to maintain longer bursts of cavitation activity, may be necessary to overcome these limitations. It may also be necessary to first use reversible focus finding methods such as thermometry or acoustic radiation force imaging to narrow in on the likely location of the bubble cloud. Once this region is located, the operator can determine the optimal set of tradeoffs to yield the best image of the bubble cloud.

This study reduces the chance of generating an appreciable acoustic radiation force or streaming by using very short pulses with a very low duty cycle. Other pulsing methods with higher duty cycles or longer pulse lengths may successfully generate a radiation force displacement or streaming effect. These motions will introduce both phase and magnitude perturbations to the signal at the focus.

We envision an MR-guided histotripsy protocol that uses sequences that apply both high and low k-space frequencies. At the start of therapy, the operator will use sequences with high k-space frequencies to verify proper placement of the bubble cloud. Then, over the course of treatment, the operator will use sequences with low k-space frequencies to monitor the disruption of the target. As the tissue is disrupted, the negative contrast in the MR images will also increase.

Conclusion

Cavitation-sensitive MR sequences can detect the incoherent, intravoxel water motion introduced by histotripsy bubble clouds formed in biologic tissue. Though, at the onset of treatment, intact tissue structures may inhibit water flow, these sequences can still capture cavitation specific contrast when their gradient waveforms enable a sufficiently high sensitivity. Sequences with very low sensitivity have difficulty observing the first bubble clouds formed in tissues. However, in this case, cavitation specific contrast may become visible as the tissue target is progressively destroyed.

References

1. Kim Y, Wang TY, Zhen X, Cain CA. Lesion generation through ribs using histotripsy therapy without aberration correction. IEEE Trans. Ultrason. Ferroelectr. Freq. Control 2011;58:2334–2343.

2. Kim Y, Vlaisavljevich E, Owens GE, Allen SP, Cain CA, Xu Z. In vivo transcostal histotripsy therapy without aberration correction. Phys. Med. Biol. 2014;59:2553–2568.

3. Vlaisavljevich E, Kim Y, Allen SP, Owens G, Pelletier S, Cain CA, Ives K, Xu Z. Image-guided non-invasive ultrasound liver ablation using histotripsy: feasibility study in an in vivo porcine model. Ultrasound Med. Biol. 2013;39:1398–1409.

4. Kim Y, Hall T, Xu Z, Cain CA. Transcranial histotripsy therapy: A feasibility study. IEEE Trans. Ultrason. Ferroelectr. Freq. Control 2014;61:582–593.

5. Alkins R, Huang Y, Pajek D, Hynynen K. Cavitation-based third ventriculostomy using MRI-guided focused ultrasound. J. Neurosurg. 2013;119:1520–1529.

6. Arvanitis CD, McDannold N. Integrated ultrasound and magnetic resonance imaging for simultaneous temperature and cavitation monitoring during focused ultrasound therapies. Med. Phys. 2013;40:112901.

7. Bigelow TA, Davis G, Avendano A, et al. Dependence of ablative ability of high-intensity focused ultrasound cavitation-based histotripsy on mechanical properties of agar. J. Acoust. Soc. Am. 2014;136:3018–3027.

8. Gyöngy M, Coussios CC. Passive spatial mapping of inertial cavitation during HIFU exposure. IEEE Trans. Biomed. Eng. 2010;57:48–56.

9. O'Reilly MA, Jones RM, Hynynen K, OReilly M, Jones RM, Hynynen K. Three-dimensional transcranial ultrasound imaging of microbubble clouds using a sparse hemispherical array. IEEE Trans. Biomed. Eng. 2014;61:1285–1294.

10. Clement GT, Hynynen K. A non-invasive method for focusing ultrasound through the human skull. Phys. Med. Biol. 2002;47:1219–1236.

11. Miller GW, Eames M, Snell J, Aubry J-F. Ultrashort echo-time MRI versus CT for skull aberration correction in MR-guided transcranial focused ultrasound: In vitro comparison on human calvaria. Med. Phys. 2015;42:2223–2233.

12. Arvanitis CD, Clement G, McDannold N. Transcranial assessment and visualization of acoustic cavitation: modeling and experimental validation. IEEE Trans. Med. Imaging 2015;34:1270–1281.

13. Khokhlova TD, Canney MS, Lee D, Marro KI, Crum LA, Khokhlova VA, Bailey MR. Magnetic resonance imaging of boiling induced by high intensity focused ultrasound. J. Acoust. Soc. Am. 2009;125:2420–2431.

14. Damianou C, Ioannides K, Hadjisavvas V, Mylonas N, Couppis A, Iosif D, Kyriacou PA. MRI monitoring of lesions created at temperature below the boiling point and of lesions created above the boiling point using high intensity focused ultrasound. J. Biomed. Sci. Eng. 2010;03:763–775.

15. Alexander AL, McCreery TT, Barrette TR, Gmitro AF, Unger EC. Microbubbles as novel pressure-sensitive MR contrast agents. Magn. Reson. Med. 1996;35:801–806.

16. Cheung JS, Chow AM, Guo H, Wu EX. Microbubbles as a novel contrast agent for brain MRI. Neuroimage 2009;46:658–664.

17. Dharmakumar R, Plewes DB, Wright GA. On the parameters affecting the sensitivity of MR measures of pressure with microbubbles. Magn. Reson. Med. 2002;47:264–273.

18. Ueguchi T, Tanaka Y, Hamada S, Kawamoto R, Ogata Y, Matsumoto M, Nakamura H, Johkoh T. Air microbubbles as MR susceptibility contrast agent at 1.5 tesla. Magn. Reson. Med. Sci. 2006;5:147–150.

19. Allen SP, Hall TL, Cain CA, Hernandez-Garcia L. Controlling cavitation-based image contrast in focused ultrasound histotripsy surgery. Magn. Reson. Med. 2015;73:204–213.

20. Lin SC, Chen CW, Wu CH, Wang CH, Kang ST, Yeh CK, Chen WS, Peng HH. Real-time monitoring of inertial cavitation effect on diluted microbubbles by MRI. In: Proceedings of the 21st Annual Meeting of ISMRM. Salt Lake City, UT; 2013. p. 1825.

21. Parsons JE, Cain CA, Fowlkes JB. Cost-effective assembly of a basic fiber-optic hydrophone for measurement of high-amplitude therapeutic ultrasound fields. J. Acoust. Soc. Am. 2006;119:1432–1440.

22. Lin KW, Kim Y, Maxwell AD, Wang TY, Hall TL, Xu Z, Fowlkes JB, Cain CA. Histotripsy beyond the intrinsic cavitation threshold using very short ultrasound pulses: microtripsy. IEEE Trans. Ultrason. Ferroelectr. Freq. Control 2014;61:251–265.

23. Branch CA, Hernandez L, Yongbi M, Huang NC, Helpern JA. Rapid and continuous monitoring of cerebral perfusion by magnetic resonance line scan assessment with arterial spin tagging. NMR Biomed. 1999;12:15–25.

24. Culjat MO, Goldenberg D, Tewari P, Singh RS. A review of tissue substitutes for ultrasound imaging. Ultrasound Med. Biol. 2010;36:861–73.

25. Vlaisavljevich E, Lin K-W, Maxwell A, et al. Effects of ultrasound frequency and tissue stiffness on the histotripsy intrinsic threshold for cavitation. Ultrasound Med. Biol. 2015;41:1651–1667.

26. Maxwell AD, Cain CA, Hall TL, Fowlkes JB, Xu Z. Probability of cavitation for single ultrasound pulses applied to tissues and tissue-mimicking materials. Ultrasound Med. Biol. 2013;39:449–465.

27. Wang TY, Xu Z, Winterroth F, Hall TL, Fowlkes JB, Rothman ED, Roberts WW, Cain CA. Quantitative ultrasound backscatter for pulsed cavitational ultrasound therapy-histotripsy. IEEE Trans. Ultrason. Ferroelectr. Freq. Control 2009;56:995–1005.

28. Roberts WW, Hall TL, Ives K, Wolf Jr JS, Fowlkes JB, Cain CA. Pulsed cavitational ultrasound: a noninvasive technology for controlled tissue ablation (histotripsy) in the rabbit kidney. J. Urol. 2006;175:734–738.

29. Wang TY, Hall TL, Xu Z, Fowlkes JB, Cain CA. Imaging feedback of histotripsy treatments using ultrasound shear wave elastography. IEEE Trans. Ultrason. Ferroelectr. Freq. Control 2012;59:1167–1181.

30. Zhang X, Miller RM, Lin K-W, Levin AM, Owens GE, Gurm HS, Cain CA, Xu Z. Real-time feedback of histotripsy thrombolysis using bubble-induced color Doppler. Ultrasound Med. Biol. 2015;41:1386–401.

31. Wang TY, Xu Z, Hall TL, Fowlkes JB, Cain CA. An efficient treatment strategy for histotripsy by removing cavitation memory. Ultrasound Med. Biol. 2012;38:753–766.

32. Kim Y, Fifer CG, Gelehrter SK, Owens GE, Berman DR, Vlaisavljevich E, Allen SP, Ladino-Torres MF, Xu Z. Developmental impact and lesion maturation of histotripsy-mediated non-invasive tissue ablation in a fetal sheep model. Ultrasound Med. Biol. 2013;39:1047–1055.

33. Hall TL, Lee GR, Hernandez L, Cain CA. Relaxation properties of cavitation induced tissue lesions. In: Proccedings of the 15th Annual Meeting of ISMRM. Berlin; 2007. p. 1118.

34. Allen SP, Roberts WW, Hall TL, Cain CA, Hernandez L. Characterization of in vivo histotripsy lesions using high field MRI. In: Proceedings of the 20th Annual Meeting of ISMRM. Melbourne; 2012. p. 1582.

35. Partanen A, Farr N, Kreider W, Khokhlova T, Maxwell A, Wang Y-N, Bailey M, Khokhlova V. Use of MRI to visualize mechanically fractionated lesions generated by boiling histotripsy in tissue. In: Abstract Book of 14th International Symposium for Therapeutic Ultrasound. Las Vegas; 2014.

Figure Captions

Fig. 1

Figure 1: Experimental setup used in this paper. A histotripsy transducer was placed in the bore of an MR scanner. A tissue sample (red, vertical rectangle) was placed at the transducer focus (ellipse). A surface coil was place about the sample and used to monitor therapy by imaging a plane transecting the focus (blue, horizontal rectangle). The cavity between the elements of the transducer and the cap was filled with degassed saline solution.

Fig. 2

Figure 2: Diagrams of histotripsy sensitized MR pulse sequences used in this study. **A**) 1-D, spin-echo, line-scan sequence. **B**). 2-D EPI sequence. Both sequences are sensitized to histotripsy by synchronizing a bipolar gradient waveform with a single, 5 μs histotripsy acoustic pulse (red arrow). Experiments were conducted by using these sequences to repeatedly image the transducer focus. Each new instance of the sequence would simultaneously apply and monitor an additional acoustic pulse to the target. Abbreviations: RF: Radio Frequency, SS: Slice Select, PE: Phase Encode, RO: Readout, US: Ultrasound.

Fig. 3

Figure 3: Slice planning for the orthogonal excitation pulse. **A**) A sacrificial sample is placed in the transducer focus. **B**) A cavitaiton-sensitized 2D sequence was used to locate the focus and plan the orthogonal refocusing plane (green lines). **C**) The refocusing slice is rotated to excited a column that transects the transducer focus. **D**) Resulting 1D line scans. The histotripsy bubble cloud creates localized signal loss that is easily detected when compared to the control case.

Comment [SPA14]: Changes made in response to comment 1 by Referee 1.

Fig. 4

Figure 4: Probability–pressure data and fitted curves obtained using the cavitation sensitized line-scan sequence and the passive cavitation detection (PCD) system. The PCD and MRI based methods show a 0.5 probability cavitation threshold at 26.4 and 26.6 MPa peak negative pressures respectively. These measurements were taken in a gel sample pre-treated with 1000 histotripsy pulses. Intact tissues, unlike the gel sample used here, may interfere with water motion and inhibit the performance of the MR sequence.

Fig. 5

Figure 5: The mean (dark line) and standard deviation (light envelope) of the motion weighted and T2-weighted signal (T2W) at the cavitation site vs the number of acoustic pulses applied to the sample. For images acquired at low spatial frequencies, signal loss caused by cavitation is not immediately differentiable from the T2-weighted signal, where cavitation-based motion is not present. However, this signal does become differentiable after several acoustic pulses are applied to the tissue target. At high spatial frequencies, cavitation specific contrast is immediately apparent and remains differentiable over the course of treatment. The T2-weighted signal in liver increases with treatment pulse number, but remains constant in brain.

Fig. 6

Figure 6: Echo-planar images (EPI) of a sample of brain tissue taken (**A**) prior to therapy, and (**B**) over the first two acoustic pulses applied to the sample. The sensitizing gradients extends to a k-space frequency of 300 cm^{-1}. The bubble clouds applied in (**B**) cause localized signal attenuation as indicated by the arrow. Dividing the image in (**B**) by the image in (**A**) isolates cavitation specific contrast and the result is shown in (**C**). The EPI sequence is able to detect and localize the first two histotripsy pulses applied to the tissue sample.

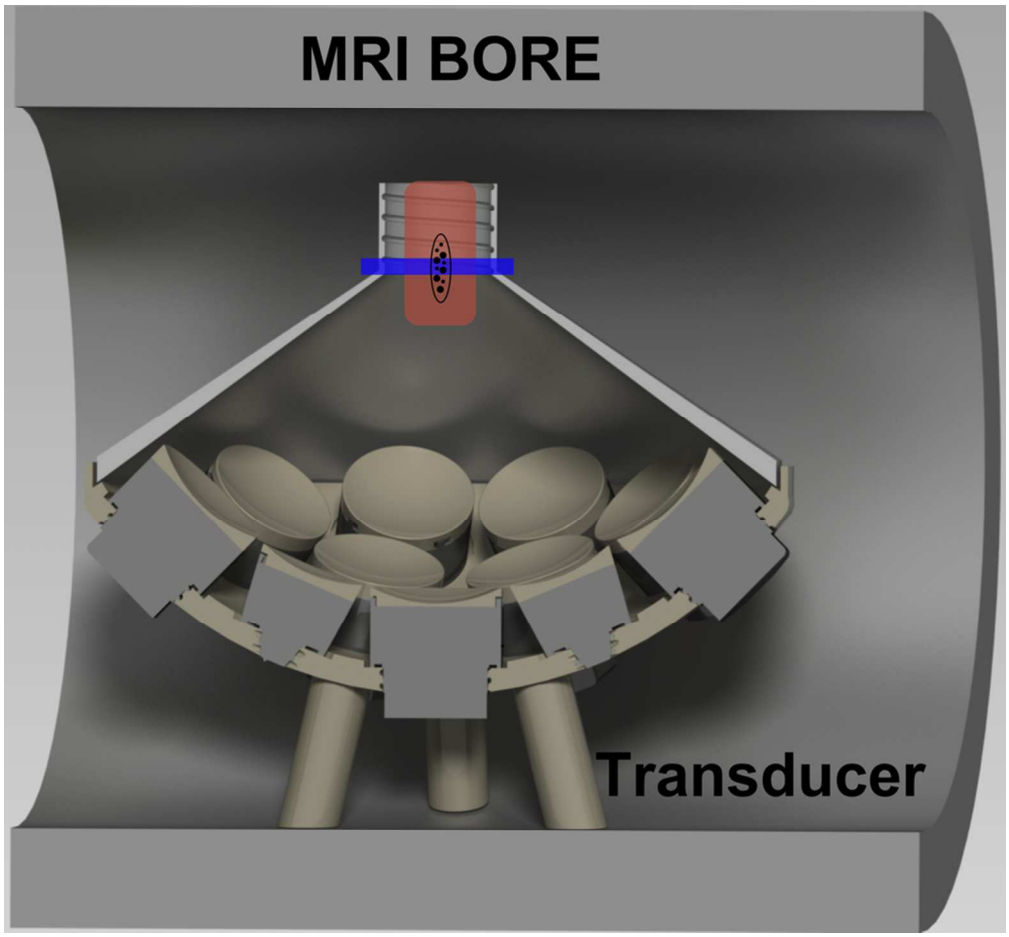

Figure 1: Experimental setup used in this paper. A histotripsy transducer was placed in the bore of an MR scanner. A tissue sample (red, vertical rectangle) was placed at the transducer focus (ellipse). A surface coil was place about the sample and used to monitor therapy by imaging a plane transecting the focus (blue, horizontal rectangle). The cavity between the elements of the transducer and the cap was filled with degassed saline solution.
80x74mm (300 x 300 DPI)

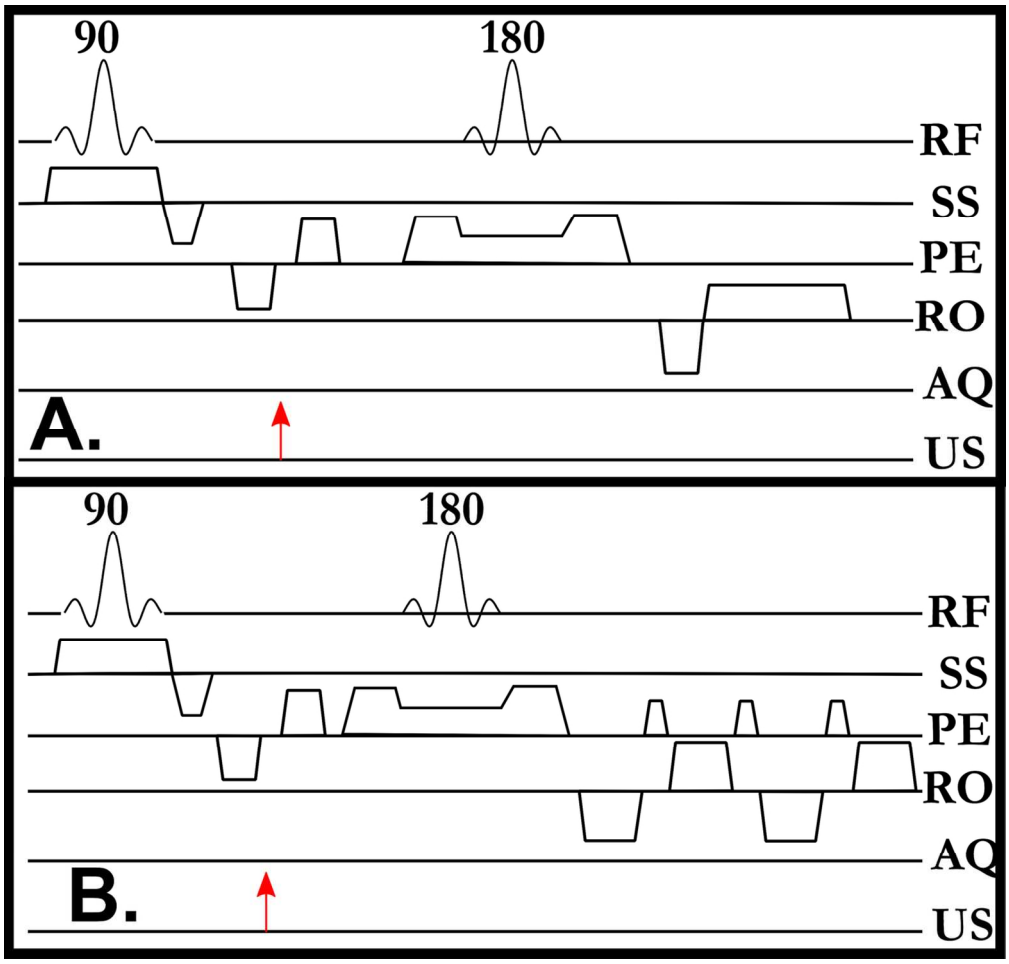

Figure 2: Diagrams of histotripsy sensitized MR pulse sequences used in this study. A) 1-D, spin-echo, line-scan sequence. B). 2-D EPI sequence. Both sequences are sensitized to histotripsy by synchronizing a bipolar gradient waveform with a single, 5 μs histotripsy acoustic pulse (red arrow). Experiments were conducted by using these sequences to repeatedly image the transducer focus. Each new instance of the sequence would simultaneously apply and monitor an additional acoustic pulse to the target. Abbreviations: RF: Radio Frequency, SS: Slice Select, PE: Phase Encode, RO: Readout, US: Ultrasound.Abbreviations: RF: Radio Frequency, SS: Slice Select, PE: Phase Encode, RO: Readout, US: Ultrasound.
123x118mm (300 x 300 DPI)

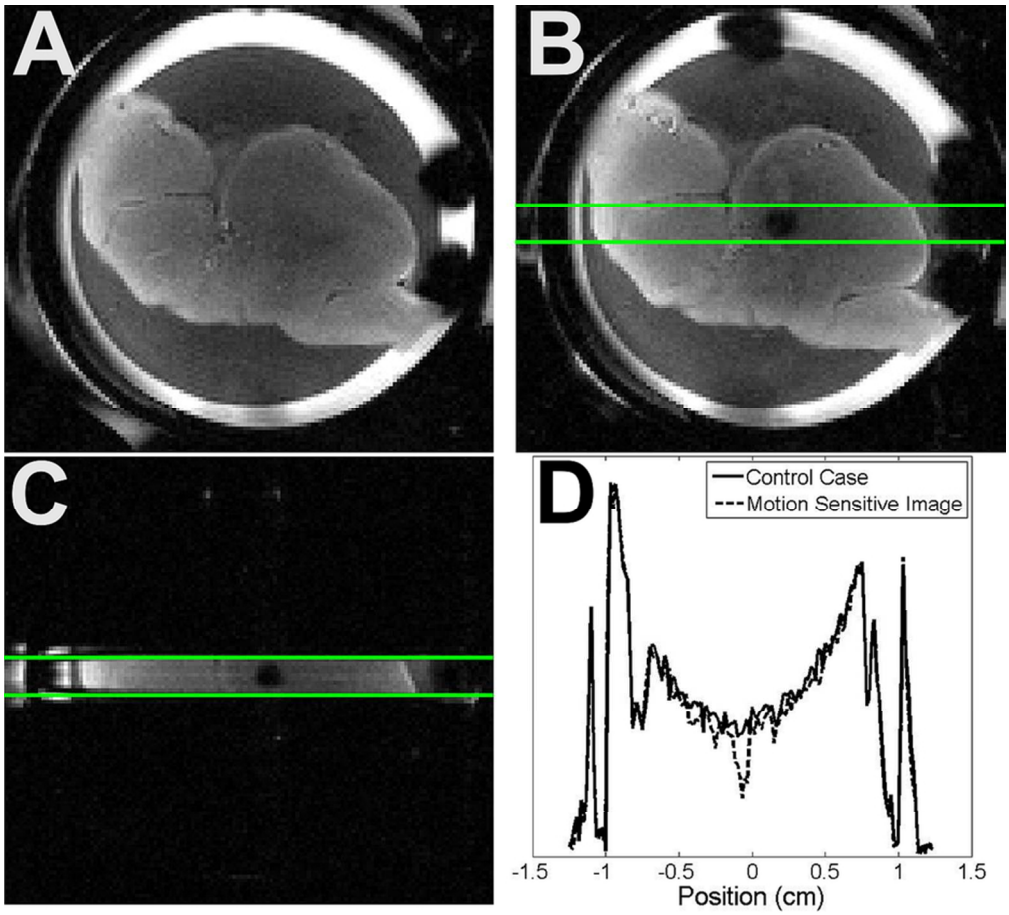

Figure 3: Slice planning for the orthogonal excitation pulse. A) A sacrificial sample is placed in the transducer focus. B) A cavitation-sensitized 2D sequence was used to locate the focus and plan the orthogonal refocusing plane (green lines). C) The refocusing slice is rotated to excited a column that transects the transducer focus. D) Resulting 1D line scans. The histotripsy bubble cloud creates localized signal loss that is easily detected when compared to the control case.
78x71mm (300 x 300 DPI)

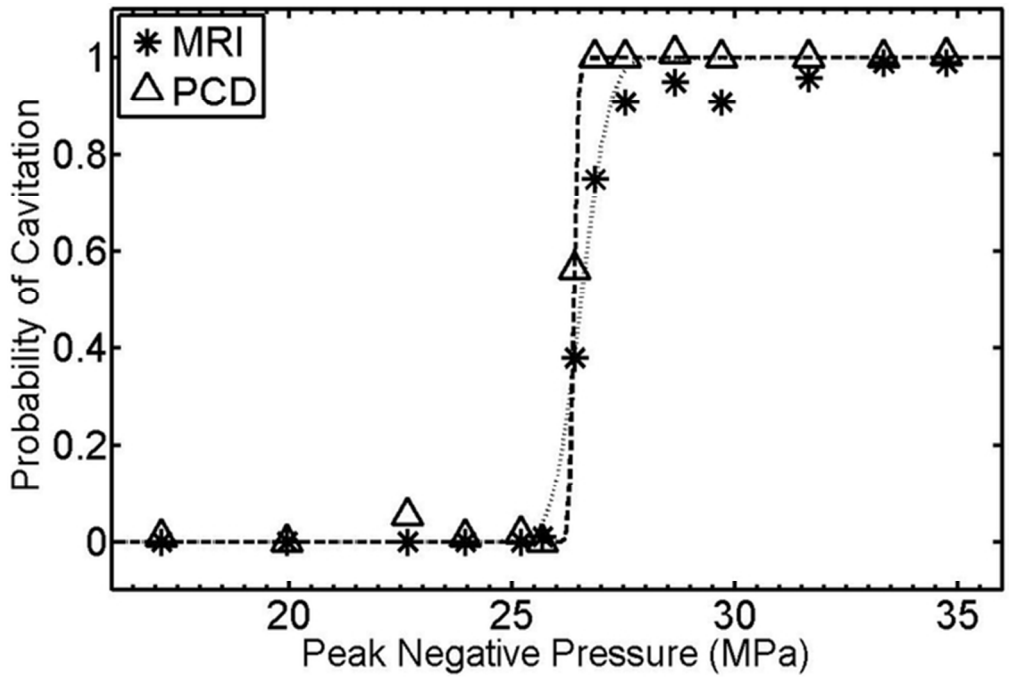

Figure 4: Probability–pressure data and fitted curves obtained using the cavitation sensitized line-scan sequence and the passive cavitation detection (PCD) system. The PCD and MRI based methods show a 0.5 probability cavitation threshold at 26.4 and 26.6 MPa peak negative pressures respectively. These measurements were taken in a gel sample pre-treated with 1000 histotripsy pulses. Intact tissues, unlike the gel sample used here, may interfere with water motion and inhibit the performance of the MR sequence.
58x39mm (300 x 300 DPI)

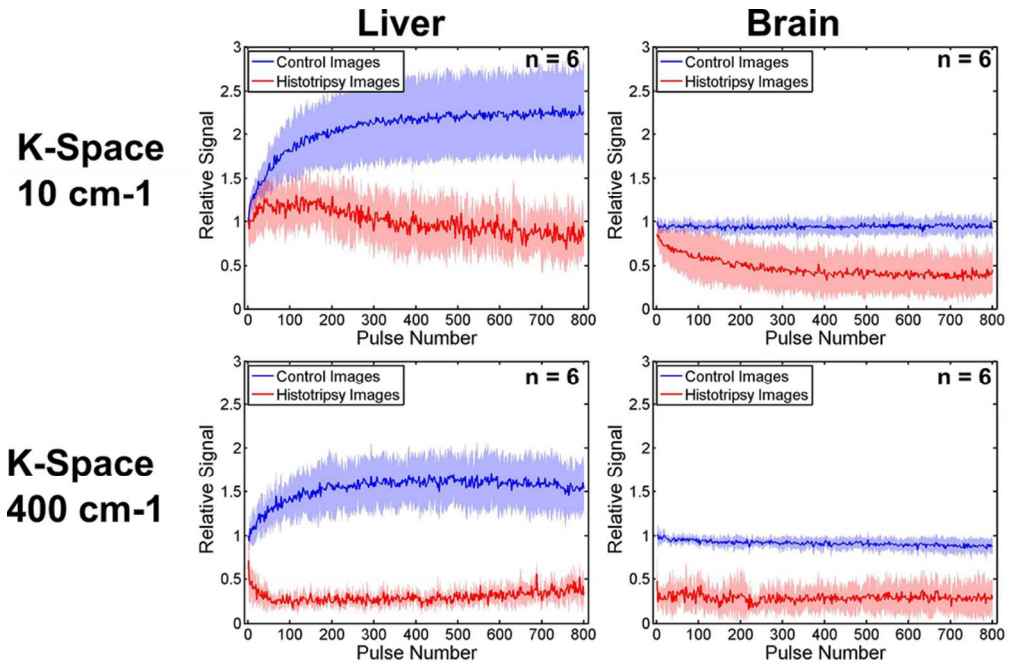

Figure 5: The mean (dark line) and standard deviation (light envelope) of the motion weighted and T2-weighted signal (T2W) at the cavitation site vs the number of acoustic pulses applied to the sample. For images acquired at low spatial frequencies, signal loss caused by cavitation is not immediately differentiable from the T2-weighted signal, where cavitation-based motion is not present. However, this signal does become differentiable after several acoustic pulses are applied to the tissue target. At high spatial frequencies, cavitation specific contrast is immediately apparent and remains differentiable over the course of treatment. The T2-weighted signal in liver increases with treatment pulse number, but remains constant in brain.
84x55mm (300 x 300 DPI)

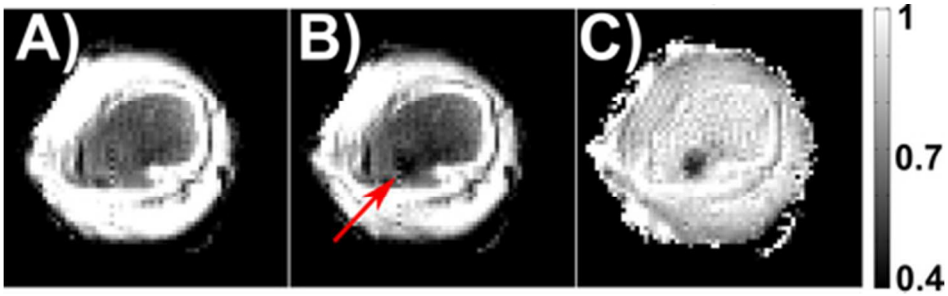

Figure 6: Echo-planar images (EPI) of a sample of brain tissue taken (A) prior to therapy, and (B) over the first two acoustic pulses applied to the sample. The sensitizing gradient extends to a k-space frequency of 300 cm-1. The bubble clouds applied in (B) cause localized signal attenuation as indicated by the arrow. Dividing the image in (B) by the image in (A) isolates cavitation specific contrast and the result is shown in (C). The EPI sequence is able to detect and localize the first two histotripsy pulses applied to the tissue sample.
39x12mm (300 x 300 DPI)